

PAPER

# Constraining gamma-ray lines from dark matter annihilation using Fermi-LAT and H.E.S.S. data




To cite this article: Lucia Angel *et al* JCAP04(2024)028

View the [article online](#) for updates and enhancements.

## You may also like

- [Dark matter in dwarf spheroidal galaxies and indirect detection: a review](#)  
Louis E Strigari
- [Gamma-ray constraints on dark-matter annihilation to electroweak gauge and Higgs bosons](#)  
Michael A. Fedderke, Edward W. Kolb, Tongyan Lin et al.
- [Constraining the Origin of the Puzzling Source HESS J1640465 and the PeVatron Candidate HESS J1641463 Using Fermi-Large Area Telescope Observations](#)  
A. Mares, M. Lemoine-Goumard, F. Acero et al.

# Constraining gamma-ray lines from dark matter annihilation using Fermi-LAT and H.E.S.S. data

Lucia Angel <sup>a,b,c</sup>, Guillermo Gambini <sup>d</sup>, Leticia Guedes <sup>a,b,c</sup>,  
Farinaldo S. Queiroz <sup>a,b,c</sup> and Vitor de Souza<sup>d</sup>

<sup>a</sup>*Departamento de Física, Universidade Federal do Rio Grande do Norte,  
59078-970, Natal, RN, Brasil*

<sup>b</sup>*International Institute of Physics, Federal University of Rio Grande do Norte,  
Campus Universitário, Lagoa Nova, Natal-RN 59078-970, Brazil*

<sup>c</sup>*Millennium Institute for Subatomic Physics at the High-Energy Frontier (SAPHIR) of ANID,  
Fernández Concha 700, Santiago, Chile*

<sup>d</sup>*Instituto de Física de São Carlos, Universidade de São Paulo,  
Av. Trabalhador São Carlense 400, São Carlos-SP, 13566-590, Brazil*

*E-mail:* [lucia.correa.717@ufrn.edu.br](mailto:lucia.correa.717@ufrn.edu.br), [guillermo.gambini@ifsc.usp.br](mailto:guillermo.gambini@ifsc.usp.br),  
[leticia.guedes.110@ufrn.edu.br](mailto:leticia.guedes.110@ufrn.edu.br), [farinaldo.queiroz@ufrn.br](mailto:farinaldo.queiroz@ufrn.br),  
[vitor@ifsc.usp.br](mailto:vitor@ifsc.usp.br)

**ABSTRACT:** Using 14 years of Fermi-LAT data and 10 years of H.E.S.S. observations in the direction of the galactic center, we derive limits on gamma-ray lines originated from dark matter annihilations for fermionic and scalar fields. We describe the dark matter annihilation into  $\gamma\gamma$  or  $\gamma Z$  final states in terms of effective operators and place limits on the energy scale as a function of the dark matter mass, taking into account the energy resolution of the instruments. For the Fermi-LAT data, we considered an NFW and a contracted NFW dark matter density profile, the latter being preferred by the Fermi GeV excess. For the H.E.S.S. observation, we used NFW and Einasto profiles. Fermi-LAT yields the most stringent constraints for dark matter masses below 300 GeV, whereas H.E.S.S. has the strongest ones for dark matter masses above 1 TeV. The telescopes share similar sensitivities for dark matter masses between 300 GeV and 1 TeV. We conclude that Fermi-LAT (H.E.S.S.) can probe energy scales up to 10(20) TeV for scalar and fermionic dark matter particles.

**KEYWORDS:** dark matter theory, gamma ray detectors

**ARXIV EPRINT:** [2311.17827](https://arxiv.org/abs/2311.17827)

---

## Contents

<b>1</b>	<b>Introduction</b>	<b>1</b>
<b>2</b>	<b>Dark matter signal</b>	<b>3</b>
<b>3</b>	<b>Effective field theory</b>	<b>4</b>
<b>4</b>	<b>Cross sections</b>	<b>4</b>
4.1	Scalar dark matter	5
4.2	Fermionic dark matter	6
<b>5</b>	<b>Results</b>	<b>7</b>
<b>6</b>	<b>Conclusions</b>	<b>8</b>

---

## 1 Introduction

The nature of dark matter has been established from several cosmological and astronomical observations, yet its nature remains unknown [1]. Numerous experimental endeavors are underway to detect non-gravitational interactions of dark matter, employing methods such as the direct detection of its scattering off nuclei and direct production in particle accelerators. An orthogonal search strategy involves the detection of the byproducts of dark matter annihilation into Standard Model (SM) particles [2]. A particularly noteworthy aspect of this search is the transparency of the Universe to gamma rays with energies around 100 GeV over galactic distances, facilitating the use of their spatial distribution and energy spectrum as tools to distinguish potential dark matter signals from often ambiguous astrophysical backgrounds [3–5].

As it is often assumed that dark matter particles interacted with SM particles in the early universe, it is reasonable to assume that such interactions might still take place today, especially in astrophysical regions which are dark matter dominated such as dwarf spheroidal galaxies. In this aspect, dark matter annihilations into SM particles will yield a continuous gamma-ray emission, which is not easily distinguished from other astrophysical emissions [6–20]. Nevertheless, dark matter annihilation into photon pairs produces monochromatic photons, which represent a smoking-gun signature of dark matter annihilation due to a relative lack of confounding astrophysical backgrounds. An eventual observation of gamma-ray lines will point to the dark matter mass, as  $E_\gamma = m_\chi$ , where  $m_\chi$  is the dark matter mass. Thus, the search for gamma-ray lines from dark matter annihilation is worth pursuing. That said, H.E.S.S. collaboration searched for gamma-ray lines in the 300 GeV–70 TeV energy range, in the central region of the Milky Way halo, which is one of the most promising targets due to the large dark matter density and its proximity to Earth. H.E.S.S. used a two-dimensional maximum likelihood method to account for the spectral and spatial features of the dark matter signal and have a better discrimination power over the background. No signal gamma-ray excess has been found during the ten years of observations, which led

Scalar Dark Matter Operators — Dimension Six		
S1	$\frac{1}{\Lambda_{S1}^2} \chi \chi^* B_{\mu\nu} B^{\mu\nu}$	$\gamma\gamma$
S2	$\frac{1}{\Lambda_{S2}^2} \chi \chi^* W_{\mu\nu}^a W^{a\mu\nu}$	$\gamma\gamma, \gamma Z$
S3	$\frac{1}{\Lambda_{S3}^2} \chi \chi^* B_{\mu\nu} \tilde{B}^{\mu\nu}$	$\gamma\gamma$
S4	$\frac{1}{\Lambda_{S4}^2} \chi \chi^* W_{\mu\nu}^a \tilde{W}^{a\mu\nu}$	$\gamma\gamma, \gamma Z$

**Table 1.** List of effective interactions for complex scalar dark matter and the type of line signals ( $\gamma\gamma$ ,  $\gamma Z$ ).

Fermion Dark Matter — Dimension 5 Operators		
F1	$\frac{1}{\Lambda_{A1}} \bar{\chi} \gamma^{\mu\nu} \chi B_{\mu\nu}$	$\gamma\gamma$
F2	$\frac{1}{\Lambda_{A2}} \bar{\chi} \gamma^{\mu\nu} \chi \tilde{B}_{\mu\nu}$	$\gamma\gamma, \gamma Z$

**Table 2.** List of effective interactions for Dirac fermion dark matter and the type of line signals ( $\gamma\gamma$ ,  $\gamma Z$ ).

to an upper bound on the dark matter annihilation cross-section into gamma-ray lines of  $4 \times 10^{-28} \text{cm}^3 \text{s}^{-1}$  for  $m_\chi = 1 \text{ TeV}$  [21] assuming the dark matter density to be distributed in the galaxy obeying an Einasto profile [22, 23]. Fermi-LAT telescope has collected over a decade of data in the direction of the galactic center [24]. Fermi-LAT collaboration has reported a search for the first 62 months of the mission in the gamma-ray energy range of 1 – 100 GeV from a  $15^\circ$  degree region centered in the GC. An updated study includes fourteen years of data with photons from 10 GeV to 2 TeV, the event selection (PASS-8), and a much larger region consisting of the inner  $30^\circ$  of our galaxy [25]. An upper bound on the dark matter annihilation cross-section into gamma-ray lines of  $6 \times 10^{-30} \text{cm}^3 \text{s}^{-1}$  was found adopted a Navarro-Frenk-White profile [26] and a contracted density profile which is preferred by the dark matter interpretation of the Fermi GeV gamma-ray excess [27]. We will use these findings to place a limit on the fermionic and scalar dark matter models that annihilate into gamma-ray lines using effective operators. A significant improvement is expected once the Cherenkov Telescope Array starts taking data [28–38]. In this study, we focus on real data and not future projections, and for this reason, we rely on Fermi-LAT and H.E.S.S. data which yield the most relevant constraints in the mass range compared to other instruments [39–41].

Therefore, our work extends previous works [42] that addressed dark matter annihilation into gamma-ray lines in the context of effective operators because we use an updated data set from both Fermi-LAT and H.E.S.S. telescope, and we consider both fermionic and scalar dark matter concluding that those searches for gamma-ray lines can probe new physics energy scales well above the 10 TeV.

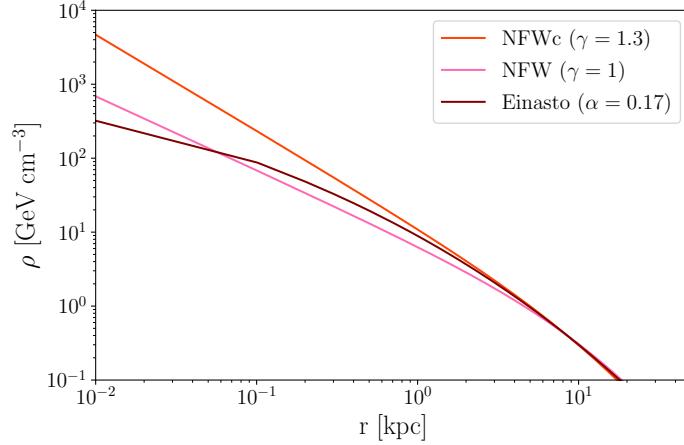


**Figure 1.** Comparison between NFW, NFW contracted (NFWc) and Einasto dark matter density profiles along the distance.

## 2 Dark matter signal

The flux of gamma-rays with energy  $E = m_\chi$  from the  $\chi\chi \rightarrow \gamma\gamma$  annihilation process in a given solid angle element of the sky ( $d\Omega$ ) is given by [43],

$$\frac{d\Phi}{d\Omega} = \frac{\langle\sigma v\rangle}{4\pi m_\chi^2} J_\Omega \mathcal{E}(E), \quad (2.1)$$

where  $\langle\sigma v\rangle$  is the velocity averaged annihilation cross-section,  $\mathcal{E}$  is effective area times exposure time, and  $J_\Omega$  the astrophysical factor defined to be,

$$\mathcal{J}(\Omega) = \int_{l.o.s} ds \rho^2(\vec{r}(s, \Omega)), \quad (2.2)$$

with  $\rho(\vec{r})$  being dark matter density along the line-of-sight (l.o.s), located at a distance  $s$  to the Earth. Using the dark matter signal given in eq. (2.1), a bound on the dark matter annihilation cross section into gamma-ray lines was derived by Fermi-LAT collaboration using  $\sim 6$  years of data [44]. In [44] three dark matter density profiles are investigated. An NFW dark matter density distribution with scale radius  $r_s = 20$  kpc normalized to a local dark matter density of  $0.4 \text{ GeV/cm}^3$  at the Earth's location, a contracted NFW profile with  $\gamma = 1.3$ , and an Einasto profile. However, in our work, we will use the updated results from [25] which, used 14 years of data assuming an NFW and a contracted NFW-like profile with  $\gamma = 1.25$  as suggested in the dark matter interpretation of the GeV Galactic Center excess [24, 27]. This contracted dark matter density profile emerges from simulations that include baryonic effects in the formation of galaxies [45, 46]. In the end, one finds a steeper dark matter density profile for the Galactic Center. We should bear in mind that alternative interpretations of the Galactic Center excess in terms of Millisecond pulsars remain viable [47–49]. Thus, the contracted NFW profile should be used with caution.

In figure 1 we plot the density as a function of the distance to the center of our galaxy for the different density profiles adopted in this work.

Besides the Fermi-LAT data, we will also use H.E.S.S. data in the direction of the galactic center. H.E.S.S. collaboration has accumulated 10 years of observations of the galactic center which represents 254 hours of exposure. In this analysis, H.E.S.S. adopted the usual ON and OFF regions to improve the signal over the background ratio. In the end, H.E.S.S. reported a limit of  $\langle\sigma v\rangle < 10^{-30} \text{cm}^3 \text{s}^{-1}$  for a 1 TeV dark matter mass.

With those limits at hand, we reinterpret them in terms of effective operators for both scalar and fermion dark matter. In the next section, we describe the effective field theory (EFT) approach used.

### 3 Effective field theory

We aim to describe the dark matter annihilation into gamma-rays using EFT. We emphasize that the EFT approach is valid under the assumption that the new physics scale is considerably larger than the effective energy scale we plan to constrain. This use of EFT method is rather old; it dates back to the beta decay description by Fermi in 1968. Moreover, we assume that the dark matter particle,  $\chi$ , to be stable via some discrete symmetry, and a singlet under the SM gauge group. We are interested in operators containing at least one photon. In principle, we expect the higher dimension operators to be subdominant as they involve additional heavy particles. One should keep in mind that there are pros and cons regarding the EFT approach. It is valid for low momentum transfer. In other words, momentum transfer is much smaller than the mediator mass that connects the dark sector and the visible one. For non-relativistic dark matter annihilation, the momentum transfer is of order to the dark matter mass. Nevertheless, the EFT represents an easy way to test dark matter models. In table 1 and table 2 we present the lowest-order effective operators that generate gamma-ray lines for scalar and fermion dark matter, respectively.

Our effective field theory is constructed as the Standard Model, plus a dark matter particle  $\chi$  which we allow to be either a complex scalar or a Dirac fermion. In case the dark matter particle is its own antiparticle, the final result will change by a factor of two. We have expressed our EFT in terms of the symmetry field, where  $W_{\mu\nu}$  and  $B_{\mu\nu}$  are the field strength tensors of the  $SU(2)_L$  and  $U(1)_Y$  groups, respectively. Consequently, in tables 1–2, the effective operators are written in terms of the symmetry fields, which after spontaneous symmetry breaking are connected to the mass eigenstates,

$$\begin{aligned} B_\mu &= A_\mu \cos \theta_W - Z_\mu \sin \theta_W \\ W_\mu^3 &= A_\mu \sin \theta_W + Z_\mu \cos \theta_W \end{aligned} \tag{3.1}$$

where  $A_\mu$  and  $Z_\mu$  are the photon and  $Z$  boson fields, respectively, and  $\theta_W$  is Weinberg mixing angle.

Up to dimension six, these effective operators represent the full list of possible annihilation channels into gamma-ray lines, and for this reason, our analysis will be restricted to them.

### 4 Cross sections

Dark matter particles should be cold today. In the galactic halo, the velocity dispersion is estimated to be  $v \sim 10^{-3}c$ . Hence, we can express the dark matter annihilation cross

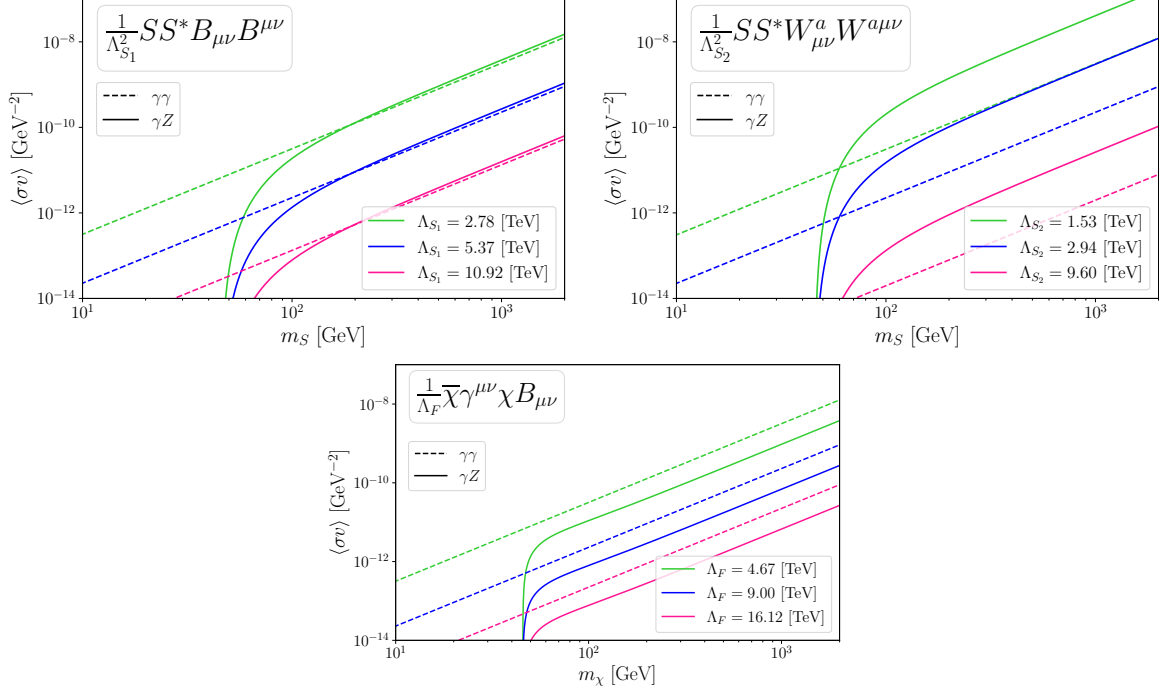


**Figure 2.** Thermally averaged annihilation cross section for scalar (S) and fermion ( $\chi$ ) dark matter annihilating into  $\gamma\gamma$  or  $\gamma Z$  for the lowest dimensional operators.

section as a series in terms of the velocity. Denoting  $p_1, p_2$  to be the incoming dark matter particle momenta,  $p_3$  and  $p_4$  will be the photon momenta. In the case of the  $\gamma Z$  line, the Z boson momentum will be represented by  $p_4$ .

The differential cross section is written

$$\frac{d\sigma}{d\Omega} = \frac{E_3}{256\pi^2 E^3 v} |\overline{\mathcal{M}}|^2 \quad (4.1)$$

where  $E = m_\chi + \mathcal{O}(v^2)$  is the energy of each dark matter particle,  $v$  is the dark matter velocity, and  $E_3 = |\vec{p}_3|$  is the energy of the outgoing line photon,  $|\mathcal{M}|^2$  is the matrix element  $\mathcal{M}$  averaged over initial dark matter spins (if any) and summed over final state particle spins.

#### 4.1 Scalar dark matter

Operators S1-S4 have the form  $\chi\chi^* F^{\mu\nu} F_{\mu\nu}$  or  $\chi\chi^* F^{\mu\nu} \tilde{F}_{\mu\nu}$ , where  $F^{\mu\nu} = B^{\mu\nu}$  or  $W^{\mu\nu}$ , and  $\chi = S$ . For the operators that involve  $F^{\mu\nu} F_{\mu\nu}$ , where  $F^{\mu\nu} = B^{\mu\nu}$  or  $W^{\mu\nu}$ , the matrix element for  $SS^* \rightarrow \gamma\gamma$  reads,

$$\mathcal{M}_{SS^* \rightarrow \gamma\gamma} = 2Y [(p_3 \cdot p_4)(\varepsilon_3 \cdot \varepsilon_4) - (p_3 \cdot \varepsilon_4)(p_4 \cdot \varepsilon_3)], \quad (4.2)$$

where  $p_i$  is the momentum of the outgoing photon with polarization vector  $\varepsilon_i$ ,  $Y \equiv \cos^2 \theta_W / \Lambda$ , and  $\theta_W$  is Weinberg angle. As a result, we get the following spin-averaged matrix element squared,

$$\sum_{\varepsilon_3, \varepsilon_4} |\mathcal{M}_{SS^* \rightarrow \gamma\gamma}|^2 = 4Y Y^\dagger \frac{s^2}{2} = \frac{2s^2 \cos^4 \theta_W}{\Lambda^4}, \quad (4.3)$$

where  $s = (p_3 + p_4)^2$ .

Fermi-LAT	$m_{S/\chi}$ [GeV]	$\frac{1}{\Lambda^2} SS^* B_{\mu\nu} B^{\mu\nu}$	$\frac{1}{\Lambda^2} SS^* W_{\mu\nu}^a W^{a\mu\nu}$	$\frac{1}{\Lambda} \bar{\chi} \gamma^{\mu\nu} \chi B_{\mu\nu}$
$\Lambda_{\min}$ [TeV]	10	2.78	1.53	4.67
	100	5.37	2.94	9.00
	1000	10.92	9.60	16.12
H.E.S.S.	$m_{S/\chi}$ [GeV]	$\frac{1}{\Lambda^2} SS^* B_{\mu\nu} B^{\mu\nu}$	$\frac{1}{\Lambda^2} SS^* W_{\mu\nu}^a W^{a\mu\nu}$	$\frac{1}{\Lambda} \bar{\chi} \gamma^{\mu\nu} \chi B_{\mu\nu}$
$\Lambda_{\min}$ [TeV]	300	6.38	5.59	9.50
	1000	12.10	10.63	17.84
	10000	18.89	16.60	27.96

**Table 3.** Lower bounds on the effective energy scale  $\Lambda$  using Fermi-LAT (NFWc) and H.E.S.S. (Einasto) data on gamma-ray lines.

For the  $SS^* \rightarrow \gamma Z$ , where  $p_4$  is the momentum of the Z boson we get,

$$\sum_{\varepsilon_e, \varepsilon_4} |\mathcal{M}_{SS^* \rightarrow \gamma Z}|^2 = 4YY^\dagger \frac{1}{2} (s - m_Z^2)^2 = \frac{2 \sin^2(2\theta_W)}{\Lambda^4} (s - m_Z^2)^2. \quad (4.4)$$

Applying these results to eq. (4.1), the average annihilation cross sections for the S1 (S3) operator into  $\gamma\gamma$  and  $\gamma Z$  lines are,

$$\langle \sigma_{SS^* \rightarrow \gamma\gamma} v_{\text{rel}} \rangle = \frac{1}{\pi} \cos^4(\theta_W) \frac{m_S^2}{\Lambda_{S1}^4}, \quad (4.5)$$

$$\langle \sigma_{SS^* \rightarrow \gamma Z} v_{\text{rel}} \rangle = \frac{1}{\pi} \sin^2(2\theta_W) \frac{m_S^2}{\Lambda_{S1}^4} \left( 1 - \frac{m_Z^2}{4m_S^2} \right)^3, \quad (4.6)$$

and for the S2 (S4) operator are,

$$\langle \sigma_{SS^* \rightarrow \gamma\gamma} v_{\text{rel}} \rangle = \frac{1}{\pi} \sin^4(\theta_W) \frac{m_S^2}{\Lambda_{S2}^4}, \quad (4.7)$$

$$\langle \sigma_{SS^* \rightarrow \gamma Z} v_{\text{rel}} \rangle = \frac{1}{\pi} \sin^2(2\theta_W) \frac{m_S^2}{\Lambda_{S2}^4} \left( 1 - \frac{m_Z^2}{4m_S^2} \right)^3. \quad (4.8)$$

## 4.2 Fermionic dark matter

In a similar vein, for operators F1 and F2, we get,

$$\langle \sigma_{\chi\bar{\chi} \rightarrow \gamma\gamma} v_{\text{rel}} \rangle = \frac{8}{\pi} \cos^4(\theta_W) \frac{m_\chi^2}{\Lambda_F^4}, \quad (4.9)$$

$$\langle \sigma_{\chi\bar{\chi} \rightarrow \gamma Z} v_{\text{rel}} \rangle = \frac{2}{\pi} \sin^2(2\theta_W) \frac{m_\chi^2}{\Lambda_F^4} \left( 1 + \frac{m_Z^2}{4m_\chi^2} \right)^2 \left( 1 - \frac{m_Z^2}{4m_\chi^2} \right), \quad (4.10)$$

for either operator. With the expressions for the annihilation cross sections, we can now place a limit on the effective energy scale  $\Lambda$  for each operator, as we do in the next section.

We plot in figure 2 the results for the average dark matter annihilation cross-section for scalar and fermionic dark matter as a function of the dark matter mass for different values of



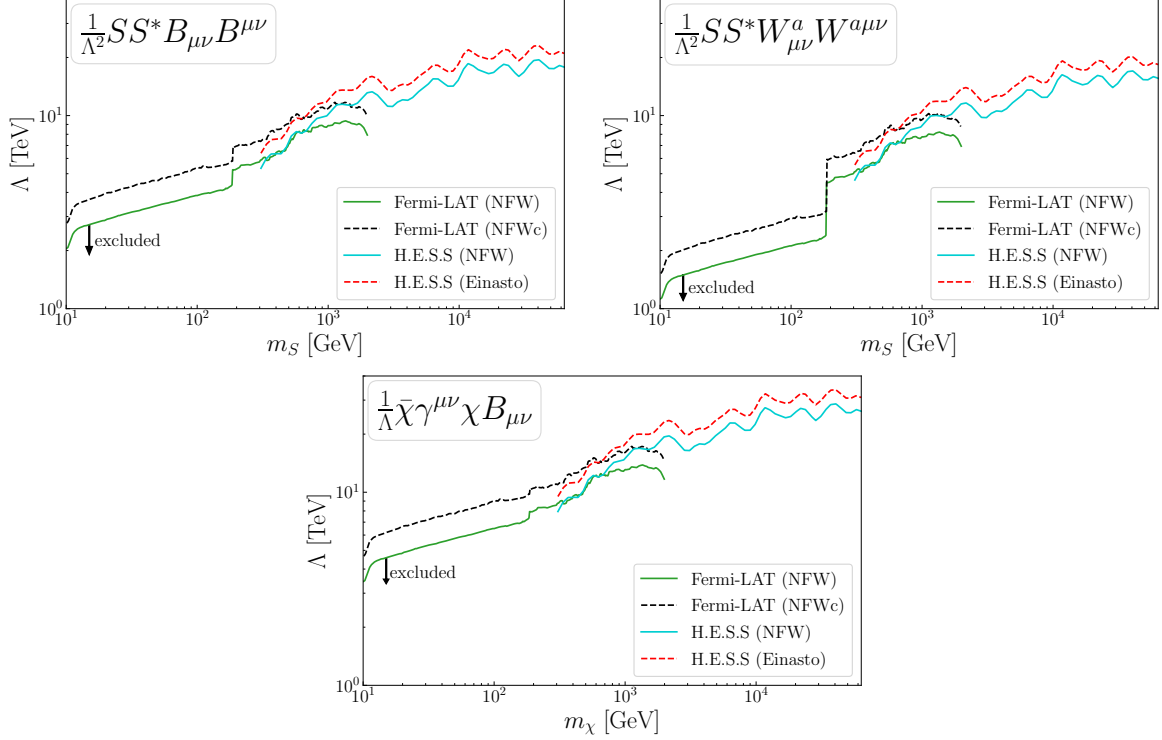


**Figure 3.** In green, lower bounds for the energy scale  $\Lambda$  with respect to the dark matter mass  $m_\chi$ . The black dashed line shows the lower limits when the DM halo profile scales as  $\rho \propto r^{-1.25}$  which is favored by the DM-annihilation interpretation of the galactic center excess. In red and cyan, we show the lower limits from H.E.S.S. 10 years of observations at the inner part of the Milky Way halo using Einasto and NFW dark matter density profiles, respectively.

A. In the upper panels, dedicated to scalar dark matter annihilating into  $\gamma\gamma$  and  $\gamma Z$  lines through the  $SS^*B_{\mu\nu}B^{\mu\nu}$ ,  $SS^*W_{\mu\nu}W^{\mu\nu}$ , we observe that the annihilation into  $B_{\mu\nu}B^{\mu\nu}$  yields a larger annihilation cross section into  $\gamma\gamma$ . For instance, taking  $m_S = 10$  GeV  $\langle\sigma v\rangle = 10^{-12}$  GeV for both operators if the effective energy scale of the operator  $SS^*B_{\mu\nu}B^{\mu\nu}$  is twice as large. This has to do with the symmetry factor that appears due to the presence of identical particles in the final state. The drop in the annihilation cross section occurs due to the term proportional to  $1 - m_Z^2/(4m_\chi^2)$  taking into account the energy resolution of the experiments that we will address below. In the bottom panel of figure 2, we focus on the fermionic case, the average annihilation cross section is larger than the scalar case. One can see that by comparing eq. (4.8) and eq. (4.10). Therefore, we have taken  $\Lambda_F = 3.4 - 13$  TeV to keep  $\langle\sigma v\rangle \simeq 10^{-12}$  GeV, for  $m_\chi = 10$  GeV.

## 5 Results

As aforementioned, we use recent searches for gamma-ray lines from dark matter annihilation using Fermi-LAT and H.E.S.S. data to constrain dark sectors through an EFT approach. As we have shown in the previous section, an effective operator can give rise to  $\gamma\gamma$  and  $\gamma Z$  lines. The  $\gamma Z$  lines happen as long as  $m_\chi > m_Z/2$ . Therefore, in general we need to

account for both  $\gamma\gamma$  and  $\gamma Z$  lines thus,

$$\langle\sigma v_{\text{rel}}\rangle_{\text{ann}} = \langle\sigma_{XX\rightarrow\gamma\gamma} v_{\text{rel}}\rangle + \langle\sigma_{XX\rightarrow\gamma Z} v_{\text{rel}}\rangle \Theta \left[ \frac{\Delta E}{E} - \frac{m_Z^2}{4m_X^2} \right], \quad (5.1)$$

where  $X$  represents a complex scalar or a Dirac fermion,  $\Delta E/E$  is the energy-dependent Fermi-LAT energy resolution, and  $\Theta$  is the Heaviside step function. The telescopes do not measure the energy of the photons with infinite precision. The finite energy resolution of the telescope, also known as energy dispersion has been encoded in the instrument response function. For Fermi-LAT, the energy resolution is  $<10\%$  between 1 GeV and 100 GeV, which is sufficient to limit the spectral distortion to less than 5% in this energy range [50]. We will assume it to be 5% throughout. The energy resolution of HESS is poorer, reading 10% [21]. Eq. (5.1) accounts for the fact that the final state photons have different energies given by,

$$E_{\gamma\gamma} = m_X, \quad (5.2)$$

$$E_{\gamma Z} = m_X - \frac{m_Z^2}{4m_X}, \quad (5.3)$$

and when their relative difference  $(E_{\gamma\gamma} - E_{\gamma Z})/E_{\gamma\gamma}$  is smaller than the energy resolution of Fermi-LAT, then the detector cannot tell the difference between the two possible final states above. We used the energy resolution of each instrument to derive the correct bound on  $\langle\sigma v\rangle$  using eq. (5.1).

That said, our results are summarized in figure 3. In figure 3 we plot the Fermi-LAT limits adopting an NFW profile and NFWc profile. As discussed previously, the NFWc density profile is more cuspy than the NFW. For this reason, the constraint on the effective energy scale that controls the dark matter annihilation cross section is stronger. We also plotted the limits from H.E.S.S. using an NFW and an Einasto profile. The importance of having both instruments is clear in figure 3. Regardless of the effective operator in question, H.E.S.S. yields the most stringent limits on the effective energy scale for dark matter masses above 1 TeV. In particular, from the leftmost upper panel, we conclude that the effective annihilation of a scalar dark matter particle annihilating into  $B_{\mu\nu}B^{\mu\nu}$  is excluded up to energy scales of 10 TeV for  $m_S = 1$  TeV, and up to 20 TeV for  $m_S \simeq 600$  TeV. H.E.S.S. loses sensitivity for dark matter masses below 300 GeV because H.E.S.S. telescopes are designed to probe very high energy gamma-rays, conversely to Fermi-LAT. Fermi-LAT is the best instrument to probe dark matter particles in the mass range between 10 GeV–300 GeV. For the fermionic case, the bound on the effective energy scale is significantly stronger because the annihilation cross section into gamma-ray lines is larger. For instance, with an NFW profile, Fermi-LAT imposes at most  $\Lambda > 2$  TeV for  $m_S = 10$  GeV, whereas  $\Lambda > 3.5$  TeV for  $m_\chi = 10$  GeV. Regardless of the dark matter nature, we notice an interesting complementarity between Fermi-LAT and H.E.S.S. for dark matter masses between 300 GeV and 1 TeV. We have explicitly summarized the strongest limits from Fermi-LAT and H.E.S.S. on the effective energy scale in table 3 which arise from adopting either an NFWc or Einasto density profile.

## 6 Conclusions

We have used 14 years of Fermi-LAT and 10 years of H.E.S.S. observations in the direction of the Galactic Center to constrain the emission of gamma-ray lines from scalar and fermionic

dark matter taking into account the energy resolution of the instruments. We have described the production of  $\gamma\gamma$  and  $\gamma Z$  lines in terms of the lowest-order effective operators, which are normalized by an effective energy scale ( $\Lambda$ ). Considering different dark matter density profiles such as NFW, NFWc, and Einasto we exhibit the Fermi-LAT and H.E.S.S. limits on  $\Lambda$  as a function of the dark matter mass. An NFWc density profile which is favored by the GeV excess observed in the Galactic center yielded stronger limits for featuring a more cuspy profile. Fermi-LAT turned out to be the best probe for dark matter masses below 300 GeV, with H.E.S.S. being more restrictive to gamma-ray lines all the way up to 600 TeV. The telescopes share similar sensitivities in the 300 GeV–1 TeV mass range. In particular, for both scalar and fermion dark matter, Fermi-LAT imposes  $\Lambda > 10$  TeV for a dark matter mass of 1 TeV, whereas H.E.S.S. places a lower limit  $\Lambda > 20$  TeV, for a 10 TeV dark matter mass.

## Acknowledgments

The authors thank Jacinto Paulo for the discussions. This work was supported by Simons Foundation (Award Number:1023171-RC), FAPESP Grant 2018/25225-9, 2021/01089-1, 2023/01197-4, ICTP-SAIFR FAPESP Grants 2021/14335-0, CNPq Grant 307130/2021-5, and ANID-Millennium Science Initiative Program ICN2019\_044. The authors acknowledge the National Laboratory for Scientific Computing (LNCC/MCTI, Brazil) for providing HPC resources of the SDumont supercomputer (<http://sdumont.lncc.br>). GG is supported by grant 2022/16580-5, São Paulo Research Foundation (FAPESP). LA acknowledges the support from Coordenação de Aperfeiçoamento de Pessoal de Nível Superior (CAPES) under grant 88887.827404/2023-00. L.G. thanks the support from Coordenação de Aperfeiçoamento de Pessoal de Nível Superior (CAPES) under grant No. 88887.704425/2022-00. VdS acknowledges CNPq grant No. 303942/2019-3.

## References

- [1] G. Bertone, D. Hooper and J. Silk, *Particle dark matter: evidence, candidates and constraints*, *Phys. Rept.* **405** (2005) 279 [[hep-ph/0404175](#)] [[INSPIRE](#)].
- [2] G. Arcadi et al., *The waning of the WIMP? A review of models, searches, and constraints*, *Eur. Phys. J. C* **78** (2018) 203 [[arXiv:1703.07364](#)] [[INSPIRE](#)].
- [3] M. Cirelli et al., *PPPC 4 DM ID: a Poor Particle Physicist Cookbook for Dark Matter Indirect Detection*, *JCAP* **03** (2011) 051 [Erratum *ibid.* **10** (2012) E01] [[arXiv:1012.4515](#)] [[INSPIRE](#)].
- [4] H.E.S.S. collaboration, *Search for a dark matter annihilation signal from the galactic center halo with H.E.S.S.*, *Phys. Rev. Lett.* **106** (2011) 161301 [[arXiv:1103.3266](#)] [[INSPIRE](#)].
- [5] T. Bringmann and C. Weniger, *Gamma ray signals from dark matter: concepts, status and prospects*, *Phys. Dark Univ.* **1** (2012) 194 [[arXiv:1208.5481](#)] [[INSPIRE](#)].
- [6] K.N. Abazajian, S. Blanchet and J.P. Harding, *Current and future constraints on dark matter from prompt and inverse-Compton photon emission in the isotropic diffuse gamma-ray background*, *Phys. Rev. D* **85** (2012) 043509 [[arXiv:1011.5090](#)] [[INSPIRE](#)].
- [7] K.N. Abazajian, P. Agrawal, Z. Chacko and C. Kilic, *Conservative constraints on dark matter from the Fermi-LAT isotropic diffuse gamma-ray background spectrum*, *JCAP* **11** (2010) 041 [[arXiv:1002.3820](#)] [[INSPIRE](#)].

- [8] T. Bringmann, F. Calore, G. Vertongen and C. Weniger, *On the relevance of sharp gamma-ray features for indirect dark matter searches*, *Phys. Rev. D* **84** (2011) 103525 [[arXiv:1106.1874](#)] [[INSPIRE](#)].
- [9] K.N. Abazajian, P. Agrawal, Z. Chacko and C. Kilic, *Lower limits on the strengths of gamma ray lines from WIMP dark matter annihilation*, *Phys. Rev. D* **85** (2012) 123543 [[arXiv:1111.2835](#)] [[INSPIRE](#)].
- [10] K.N. Abazajian and J.P. Harding, *Constraints on WIMP and Sommerfeld-enhanced dark matter annihilation from HESS observations of the galactic center*, *JCAP* **01** (2012) 041 [[arXiv:1110.6151](#)] [[INSPIRE](#)].
- [11] FERMI-LAT collaboration, *Searching for dark matter annihilation from Milky Way dwarf spheroidal galaxies with six years of Fermi Large Area Telescope data*, *Phys. Rev. Lett.* **115** (2015) 231301 [[arXiv:1503.02641](#)] [[INSPIRE](#)].
- [12] M.G. Baring, T. Ghosh, F.S. Queiroz and K. Sinha, *New limits on the dark matter lifetime from dwarf spheroidal galaxies using Fermi-LAT*, *Phys. Rev. D* **93** (2016) 103009 [[arXiv:1510.00389](#)] [[INSPIRE](#)].
- [13] C. Garcia-Cely and A. Ibarra, *Novel gamma-ray spectral features in the inert doublet model*, *JCAP* **09** (2013) 025 [[arXiv:1306.4681](#)] [[INSPIRE](#)].
- [14] F.S. Queiroz, C.E. Yaguna and C. Weniger, *Gamma-ray limits on neutrino lines*, *JCAP* **05** (2016) 050 [[arXiv:1602.05966](#)] [[INSPIRE](#)].
- [15] S. Profumo, F.S. Queiroz and C.E. Yaguna, *Extending Fermi-LAT and H.E.S.S. limits on gamma-ray lines from dark matter annihilation*, *Mon. Not. Roy. Astron. Soc.* **461** (2016) 3976 [[arXiv:1602.08501](#)] [[INSPIRE](#)].
- [16] H.E.S.S. collaboration, *Search for dark matter annihilations towards the inner galactic halo from 10 years of observations with H.E.S.S.*, *Phys. Rev. Lett.* **117** (2016) 111301 [[arXiv:1607.08142](#)] [[INSPIRE](#)].
- [17] S. Profumo, F.S. Queiroz, J. Silk and C. Siqueira, *Searching for secluded dark matter with H.E.S.S., Fermi-LAT, and Planck*, *JCAP* **03** (2018) 010 [[arXiv:1711.03133](#)] [[INSPIRE](#)].
- [18] F.S. Queiroz and C. Siqueira, *Search for semi-annihilating dark matter with Fermi-LAT, H.E.S.S., Planck, and the Cherenkov Telescope Array*, *JCAP* **04** (2019) 048 [[arXiv:1901.10494](#)] [[INSPIRE](#)].
- [19] K.N. Abazajian et al., *Strong constraints on thermal relic dark matter from Fermi-LAT observations of the galactic center*, *Phys. Rev. D* **102** (2020) 043012 [[arXiv:2003.10416](#)] [[INSPIRE](#)].
- [20] C. Siqueira, G.N. Fortes, A. Viana and F.S. Queiroz, *Indirect searches for secluded dark matter*, *PoS ICRC2021* (2021) 577 [[arXiv:2107.04053](#)] [[INSPIRE](#)].
- [21] HESS collaboration, *Search for  $\gamma$ -ray line signals from dark matter annihilations in the inner galactic halo from 10 years of observations with H.E.S.S.*, *Phys. Rev. Lett.* **120** (2018) 201101 [[arXiv:1805.05741](#)] [[INSPIRE](#)].
- [22] A.W. Graham et al., *Empirical models for dark matter halos. I. Nonparametric construction of density profiles and comparison with parametric models*, *Astron. J.* **132** (2006) 2685 [[astro-ph/0509417](#)] [[INSPIRE](#)].
- [23] J.F. Navarro et al., *The diversity and similarity of cold dark matter halos*, *Mon. Not. Roy. Astron. Soc.* **402** (2010) 21 [[arXiv:0810.1522](#)] [[INSPIRE](#)].

- [24] FERMI-LAT collaboration, *Fermi-LAT observations of high-energy  $\gamma$ -ray emission toward the galactic center*, *Astrophys. J.* **819** (2016) 44 [[arXiv:1511.02938](#)] [[INSPIRE](#)].
- [25] J.W. Foster et al., *Search for dark matter lines at the galactic center with 14 years of Fermi data*, *Phys. Rev. D* **107** (2023) 103047 [[arXiv:2212.07435](#)] [[INSPIRE](#)].
- [26] J.F. Navarro, C.S. Frenk and S.D.M. White, *The structure of cold dark matter halos*, *Astrophys. J.* **462** (1996) 563 [[astro-ph/9508025](#)] [[INSPIRE](#)].
- [27] T. Daylan et al., *The characterization of the gamma-ray signal from the central Milky Way: a case for annihilating dark matter*, *Phys. Dark Univ.* **12** (2016) 1 [[arXiv:1402.6703](#)] [[INSPIRE](#)].
- [28] H. Silverwood, C. Weniger, P. Scott and G. Bertone, *A realistic assessment of the CTA sensitivity to dark matter annihilation*, *JCAP* **03** (2015) 055 [[arXiv:1408.4131](#)] [[INSPIRE](#)].
- [29] M. Pierre, J.M. Siegal-Gaskins and P. Scott, *Sensitivity of CTA to dark matter signals from the galactic center*, *JCAP* **06** (2014) 024 [Erratum *ibid.* **10** (2014) E01] [[arXiv:1401.7330](#)] [[INSPIRE](#)].
- [30] V. Lefranc, E. Moulin, P. Panci and J. Silk, *Prospects for annihilating dark matter in the inner galactic halo by the Cherenkov Telescope Array*, *Phys. Rev. D* **91** (2015) 122003 [[arXiv:1502.05064](#)] [[INSPIRE](#)].
- [31] F.S. Queiroz and C.E. Yaguna, *The CTA aims at the inert doublet model*, *JCAP* **02** (2016) 038 [[arXiv:1511.05967](#)] [[INSPIRE](#)].
- [32] C. Garcia-Cely, M. Gustafsson and A. Ibarra, *Probing the inert doublet dark matter model with Cherenkov telescopes*, *JCAP* **02** (2016) 043 [[arXiv:1512.02801](#)] [[INSPIRE](#)].
- [33] A. Ibarra et al., *On the sensitivity of CTA to gamma-ray boxes from multi-TeV dark matter*, *JCAP* **09** (2015) 048 [Erratum *ibid.* **06** (2016) E02] [[arXiv:1503.06797](#)] [[INSPIRE](#)].
- [34] CTA CONSORTIUM collaboration, *Science with the Cherenkov Telescope Array*, World Scientific, Singapore (2018) [[DOI:10.1142/10986](#)] [[INSPIRE](#)].
- [35] CTA collaboration, *Sensitivity of the Cherenkov Telescope Array to a dark matter signal from the galactic centre*, *JCAP* **01** (2021) 057 [[arXiv:2007.16129](#)] [[INSPIRE](#)].
- [36] G. N. Fortes, F. S. Queiroz, C. Siqueira and A. Viana, *Present and future constraints on secluded dark matter in the galactic halo with TeV gamma-ray observatories*, *JCAP* **07** (2023) 043 [[arXiv:2212.05075](#)] [[INSPIRE](#)].
- [37] CHERENKOV TELESCOPE ARRAY collaboration, *Sensitivity of the Cherenkov Telescope Array to TeV photon emission from the Large Magellanic Cloud*, *Mon. Not. Roy. Astron. Soc.* **523** (2023) 5353 [[arXiv:2305.16707](#)] [[INSPIRE](#)].
- [38] CTA CONSORTIUM collaboration, *Prospects for  $\gamma$ -ray observations of the Perseus galaxy cluster with the Cherenkov Telescope Array*, [arXiv:2309.03712](#) [[INSPIRE](#)].
- [39] MAGIC and FERMI-LAT collaborations, *Limits to dark matter annihilation cross-section from a combined analysis of MAGIC and Fermi-LAT observations of dwarf satellite galaxies*, *JCAP* **02** (2016) 039 [[arXiv:1601.06590](#)] [[INSPIRE](#)].
- [40] E-ASTROGAM collaboration, *Science with e-ASTROGAM: a space mission for MeV–GeV gamma-ray astrophysics*, *JHEAp* **19** (2018) 1 [[arXiv:1711.01265](#)] [[INSPIRE](#)].
- [41] A. Acharyya et al., *Search for ultraheavy dark matter from observations of dwarf spheroidal galaxies with VERITAS*, *Astrophys. J.* **945** (2023) 101 [[arXiv:2302.08784](#)] [[INSPIRE](#)].
- [42] A. Rajaraman, T.M.P. Tait and D. Whiteson, *Two lines or not two lines? That is the question of gamma ray spectra*, *JCAP* **09** (2012) 003 [[arXiv:1205.4723](#)] [[INSPIRE](#)].

- [43] J.M. Gaskins, *A review of indirect searches for particle dark matter*, *Contemp. Phys.* **57** (2016) 496 [[arXiv:1604.00014](#)] [[INSPIRE](#)].
- [44] FERMI-LAT collaboration, *Updated search for spectral lines from galactic dark matter interactions with pass 8 data from the Fermi Large Area Telescope*, *Phys. Rev. D* **91** (2015) 122002 [[arXiv:1506.00013](#)] [[INSPIRE](#)].
- [45] P.F. Hopkins et al., *FIRE-2 simulations: physics versus numerics in galaxy formation*, *Mon. Not. Roy. Astron. Soc.* **480** (2018) 800 [[arXiv:1702.06148](#)] [[INSPIRE](#)].
- [46] C. Dessert et al., *Higgsino dark matter confronts 14 years of Fermi  $\gamma$ -ray data*, *Phys. Rev. Lett.* **130** (2023) 201001 [[arXiv:2207.10090](#)] [[INSPIRE](#)].
- [47] R.T. Bartels, T.D.P. Edwards and C. Weniger, *Bayesian model comparison and analysis of the galactic disc population of gamma-ray millisecond pulsars*, *Mon. Not. Roy. Astron. Soc.* **481** (2018) 3966 [[arXiv:1805.11097](#)] [[INSPIRE](#)].
- [48] L.J. Chang et al., *Characterizing the nature of the unresolved point sources in the galactic center: an assessment of systematic uncertainties*, *Phys. Rev. D* **101** (2020) 023014 [[arXiv:1908.10874](#)] [[INSPIRE](#)].
- [49] M. Buschmann et al., *Foreground mismodeling and the point source explanation of the Fermi galactic center excess*, *Phys. Rev. D* **102** (2020) 023023 [[arXiv:2002.12373](#)] [[INSPIRE](#)].
- [50] FERMI-LAT collaboration, *Pass 8: toward the full realization of the Fermi-LAT scientific potential*, [arXiv:1303.3514](#) [[INSPIRE](#)].